PCCP

Accepted Manuscript

ROYAL SOCIETY OF CHEMISTRY

www.rsc.org/pccp

PCCP Paper

Novel Pyrromethene dyes with N-ethyl carbazole at *meso* position: comprehensive photophysical, lasing, photostability and TD-DFT study†

Received 00th January 20xx,
Accepted 00th January 20xx

DOI: 10.1039/x0xx00000x

www.rsc.org/

Kishor G. Thorat,[a] Priyadarshani Kamble,[b] Alok K. Ray*[b] and N. Sekar*[a]

Two novel BODIPY (pyrromethene, PM) dyes containing N-ethyl carbazole at *meso* position are synthesized and their photophysical properties in different solvents and the photochemical stabilities and laser performances in n-heptane are investigated. The n-heptane solution of the dyes was used as gain media in a constructed narrow band dye laser, pumped by a Q-switched (10 Hz) frequency-doubled (532 nm) Nd:YAG laser and the results gave enhanced photo stabilities and similar peak efficiencies of the synthesized dyes as compared to parent dye PM567. When substituted at *meso* position with N-alkyl carbazole, photostability is found to be increased in comparison to PM567, and also when substituted at 2- and 6-postions with benzyl group instead of ethyl group along with N-ethyl carbazole at *meso* position, the photo stability is further increased in n-heptane. A comprehensive study on structural, photophysical and electronic properties of dyes by means of DFT and TD-DFT in the solvents of various polarities has revealed remarkable characteristics of the BODIPY chrompohore.

Introduction

The BODIPYs, (4,4-difluoro-4-bora-3a,4a-diaza-s-indacene) are highly fluorescent dyes and can be used for such diverse applications as bio-labels,[1] sensitizers in solar cells,[2] fluorescent sensors,[3–6] molecular photonic wires[7] and electron transfer reagents.[8] They exhibit low intersystem crossing (ISC) rates and often possess a triplet-triplet absorption coefficients about five times less than that of the rhodamine dyes over the laser spectral region,[7,9–16] and hence are very useful in dye laser applications. These dyes exhibit good solubility in many organic solvents and even in methyl methacrylate (MMA) that is useful for solid-state dye laser applications.[17–23] Two major inherent deficiencies of the BODIPY dyes are their small Stokes shift, known to be responsible for the ground state absorption loss leading to the reduced lasing efficiency of the PM dyes, and the fast degradation of dye molecules when used in alcohol media under lasing conditions. The problem has been addressed to some extent by carrying out modifications either at *meso* (C8) position, C3, C5 center or at the boron atom of pyrromethene moiety,[24–28] particularly for widely used PM567 (refer Fig. 1 for molecular structure of PM 567). As far as the high-average power laser applications of PM dyes are concerned, one needs to focus more on their sustainable operation and thus photochemical stability in addition to high conversion efficiency. It is now well established that photodegradation of the PM dyes occur primarily due to their photochemical reaction with *in situ* generated singlet oxygen ($^1O_2$).[29–31] It was envisaged that the photostability and lasing properties of the PM dyes can be improved by suitable modifications of the substitution pattern on the PM core. Earlier, similar approaches have been adopted to synthesize a host of analogues of the most extensively used pyrromethene dye, PM567, by incorporating different substituents at C-8 and/or C-2 + C-6 positions (Fig. 1) of the PM moiety.[9,31] Among these, PM650 (with CN at C-8) showed ~50 times higher photostability than PM567.[31] However, either the fluorescence quantum yield or Stokes shift of these analogues were too low to be used as laser dyes.[9,28] In contrast, the effect of alteration of the alkyl substituent at the pyrrole rings (C2, C3, C5, C6 positions) was much less on photophysical properties of PM dyes.[29]

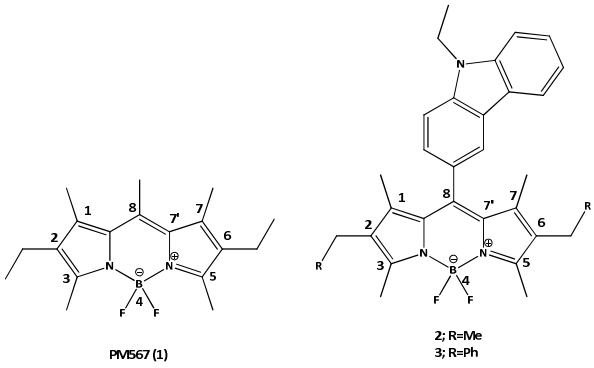

Fig. 1 Chemical structures of the widely used PM567 laser dye (**1**) and novel PM dyes (**2** and **3**).

[a]*Dyestuff Technology Department, Institute of Chemical Technology, Mumbai-400019 (India)*
[b]*Laser & Plasma Technology Division Bhabha Atomic Research Centre, Mumbai-400085 (India).*

†Electronic Supplementary Information (ESI) available: [Mulliken charge density table and optimized geometry of the dyes, Schematic representation of the Nd:YAG laser pumped constructed dye laser setup used for obtaining tunable laser efficiency of dyes. Plausible reaction mechanism of the dyes with generated singlet oxygen. ^{1}H and ^{13}C NMR, MS and/HRMS spectra of the intermediates and dyes. These materials are available free of charge via the Internet]. See DOI: 10.1039/x0xx00000x

Conversely for photostability, it is now well established that the excited dye in its triplet state is mainly responsible for the *in situ* generation of reactive singlet oxygen ($^1O_2$). The involvement of triplet excited state (T_1) of the dye has been confirmed from their higher decomposition rates in the presence of benzophenone, a triplet sensitizer.[32] Also under lasing conditions generated singlet oxygen ($^1O_2$) reacts at C7'-C8 double bond of the dye molecule which produces an unstable peroxo compound leading to the breakdown of the PM chromophore.[28,33,34] The enhanced photostability of the PM dyes in de-oxygenated dye solutions, and also in the presence of 1 wt% of singlet oxygen quenchers like Tin770, TBP, and DABCO confirmed the involvement of the singlet oxygen($^1O_2$) in the degradation of the PM molecules and thereby progressively decreasing the laser efficiency over a period of operating time.[33] Therefore, the photostability of the PM dyes might be increased by reducing the generation of reactive $^1O_2$ and/or reducing rate of reaction of dyes with $^1O_2$ in dye-solvent environment.

It was felt that if one judiciously changes the substituents at C8 or C2 + C6, chances of getting enhanced photostability of the PM dyes will be more compared to the parent dye PM567. The primary aim of the present investigation was to develop a highly photostable congener of PM567 laser dye by rational design and evaluate its photophysical, laser efficiency and photostability in comparison to the parent dye. It is a well-known fact, that carbazole derivatives owing to its good electron donor capacity have been used in various photovoltaic, OLEDs, and photo sensitizers applications.[35,36] Carbazole can be easily functionalized and its derivatives exhibit good absorption and emission properties, therefore, it has become popular among the chemists.[37–42] Recently, there is a report on the effect of insertion of carbazole group on the photophysical properties of the BODIPY dyes when there is no methyl groups at 1 and 7-positions of the PM core.[43] We wanted to evaluate the effect of the N-ethyl carbazole at meso position in the presence of 1 and 7-methyl groups on electrochemical, photophysical, laser and photostability characteristics of the PM dyes. N-Ethyl carbazole moiety at meso position was expected to be oriented orthogonally in the presence of 1 and 7-methyl groups on the PM core and should not alter the photophysical properties of the PM dyes but may change the electronic properties to some extent as a result of charge transfer from electron rich N-ethyl carbazole to electron deficient PM core. Also, it was envisaged that the change in ethyl to benzyl groups at 2 and 6-postions in combination of N-ethyl carbazole at C-8 of PM core should further alter the electrochemical properties of the PM dye leaving photophysical properties unaltered. To this end, we have synthesized two new BODIPY dyes, dye **2**, using N-ethyl carbazole aldehyde and kryptopyrrole, and dye **3**, using N-ethyl carbazole aldehyde and benzyl pyrrole,[44] compared their photophysical, lasing properties and photochemical stability with that of parent PM567 (dye **1**), and rationalized the results in terms of their photophysical properties as well as TD-DFT computations using the functional B3LYP and 6-31G(d) basis set. The molecular structures of the PM dyes **1**, **2** and **3** are illustrated in Fig. **1**.

Results and Discussion

Photophysical Characteristics. The measured photophysical parameters (longest wavelength absorption maxima (λ_{abs}), emission maxima (λ_{em}), quantum yield of fluorescence (ϕ_{fl}), and fluorescence life time (τ)) along with calculated radiative decay (k_r) and non-radiative decay (k_{nr}) rates of the dyes **2** and **3** relative to those of the dye **1** in solvents of different polarities, inclusive of practically useful solvents such as ethanol and n-heptane, for high power dye lasers (see Lasing section), are presented in Table 1. The absorption and emission spectra of the new PM dyes **2** and **3** in various solvents are shown in Figs. S1-S4 (ESI†), respectively. For illustration, the absorption and fluorescence spectra of the dyes **1**–**3** in n-heptane are shown in Figs. 2 and 3, respectively. The PM dyes **1**-**3** in n-heptane had intense $S_0 \rightarrow S_1$ absorption maxima centered at 518–523 nm, each with a smaller fwhm (full width at half maxima), 765-957 cm^{-1} in comparison to that of PM567. The wider fwhm of absorption and particularly of fluorescence spectra of the laser dyes are beneficial to provide higher laser wavelength coverage by a single dye.

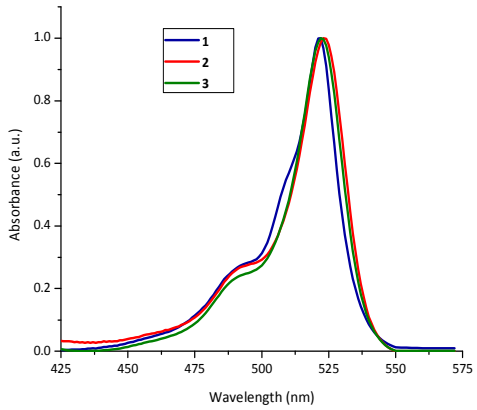

Fig. 2 Normalized longest wavelength absorption band of the PM dyes **1**-**3** in n-heptane

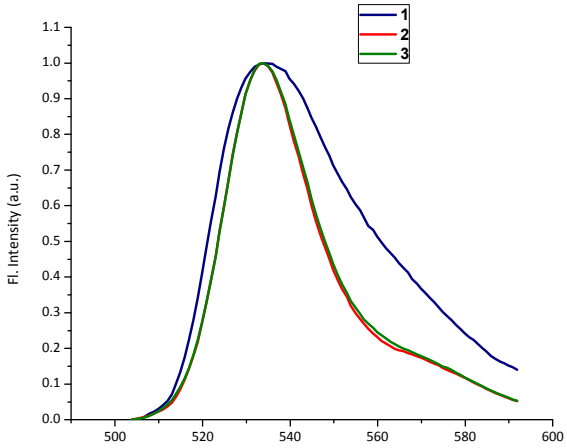

Fig. 3 Normalized emission spectra of the dyes **1-3** in n-heptane, excitation wavelength was 490 nm.

Table 1 Experimental photophysical parameters of the PM dyes **1-3** in various solvents

Solvent	λ_{abs} [a]	fwhm [b]		λ_{em} [c]	fwhm [d]		$\Delta\nu$ [e]		$\varepsilon_{max}x10^4$	ϕ_{fl} [g]	τ	$k_r x10^8$	$k_{nr}x10^8$
	nm	nm	cm^{-1}	nm	nm	cm^{-1}	nm	cm^{-1}	$M^{-1}cm^{-1}$[f]		(ns) [h]	(s^{-1}) [i]	(s^{-1}) [j]
Dye 1													
Ethanol	518	25.3	957	533	41.5	1425	15	543	8.1 [k]	0.84 [k]	6.19	1.36	0.258
n-Heptane	523	21.5	802	534	40.4	1381	11	394	9.1	0.98	6.03	1.63	0.033
Dye 2													
MeCN	519	24.3	907	533	25.2	885	14	506	7.69	0.72	n. d.	n. d.	n. d.
DMF	522	23.7	875	535	24.6	857	13	465	7.26	0.82	n. d.	n. d.	n. d.
MeOH	519	23.1	861	532	24.9	874	13	471	7.17	0.76	n. d.	n. d.	n. d.
EtOH	521	23.7	877	533	24.4	869	12	432	10.55	0.86	5.9	1.46	0.237
Acetone	519	24.6	915	532	23.4	823	13	471	7.14	0.82	n. d.	n. d.	n. d.
EtOAc	521	23.6	876	532	24.8	868	11	397	9.95	0.87	n. d.	n. d.	n. d.
$CHCl_3$	526	23.1	842	537	24.9	857	11	389	11.33	0.74	n. d.	n. d.	n. d.
1,4-dioxane	523	22.7	836	535	25.2	877	12	429	11.02	0.85	n. d.	n. d.	n. d.
n-Heptane	523	21.1	777	535	24.3	821	12	429	8.99	0.98	5.32	1.84	0.037
Dye 3													
MeCN	520	23.4	877	532	25.6	902	12	434	10.83	0.62	n. d.	n. d.	n. d.
DMF	522	24.3	879	534	22.9	802	12	430	10.73	0.69	n. d.	n. d.	n. d.
MeOH	520	22.9	854	532	24.6	867	12	434	12.91	0.72	n. d.	n. d.	n. d.
EtOH	521	22.2	823	532	25.2	879	11	397	13.66	0.83	5.38	1.54	0.316
Acetone	521	21.8	844	531	24.7	867	10	361	12.36	0.67	n. d.	n. d.	n. d.
EtOAc	520	22.6	840	532	24.3	855	12	434	11.78	0.91	n. d.	n. d.	n. d.
$CHCl_3$	524	21.4	779	535	24.9	862	11	392	15.51	0.83	n. d.	n. d.	n. d.
1,4-dioxane	522	22.2	821	533	25.5	879	11	395	16.07	0.89	n. d.	n. d.	n. d.
n-Heptane	522	20.8	766	532	24.7	837	10	360	16.03	0.89	4.99	1.76	0.220

[a]Wavelength at absorption maximum; [b]Fwhm of the absorption spectra; [c]Wavelength at emission maximum; [d]Fwhm of the emission spectra; [e]Stokes shift; [f]Molar extinction coefficient at absorption maximum wavelength; [g]Fluorescence quantum yield, determined using PM567 in ethanol (ϕ_{fl}=0.84) as standard; [h]Fluorescence life time; [i]Radiative decay rate; [j]Non-radiative decay rate; [k]Values taken from the reference;[18] n. d.=not determined.

On the other hand in case of BODIPY laser dyes, their small Stokes shift (10-15 nm) and broader fwhm of absorption and emission bands may give a larger extent of spectral overlap leading to the increase in ground state absorption of dye laser signal and thus decreased dye laser efficiency. However, the change in solvent polarities had weak influence on the fwhm and other important photophysical properties of the BODIPY chromophores, **2** and **3**, Table 1 and Figs. S1-S4 (ESI†).

The shapes of the absorption spectra of the dyes **2** and **3** were similar to that of the dye **1**, but the maxima were bathochromically shifted by 2-4 nm. The dyes **2** and **3** compared to the dye **1** showed sharper absorption bands, the fwhm decreased from 957 cm^{-1} for the dye **1** to 877 cm^{-1} and 823 cm^{-1} for the dyes **2** and **3** in ethanol, respectively. Similarly in n-heptane there was a decrease in fwhm from 802 cm^{-1} for the dye **1** to 777 cm^{-1} and 766 cm^{-1} for the dyes **2** and **3,** respectively, indicating the effect of N-ethyl carbazole at *meso* position as well as substitution of benzyl groups at 2 and 6-positions of BODIPY fluorophores further making the absorption band more intense and sharper. Similarly there is a decrease in fwhm in case of the dye **3** but the effect of N-ethyl carbazole (dye **2**) is more prominent compared to that of N-ethyl carbazole in combination with benzyl groups at 2 and 6-positions (dye **3**). The sharpening of the absorption and fluorescence bands

incase of the dyes **2** and **3** compared to the dye **1** can be attributed to significantly higher polarizability of the dye chromophore due to the increased π electron density.The fluorescence spectra of the dyes **2** and **3** were also identical throughout the series of various solvents and entirely consistent with fluorescence from the PM sub unit and are almost mirror images of the respective absorption spectra (Figs. S1-S4 (ESI†)) with a small Stokes shift (11-14 nm). This may be correlated to the minimum change in the geometry of the molecules in its excited state relative to that of respective ground state. From this it can be seen that the substitution at *meso* position has very low or negligible influence on the photophysics of the BODIPY chromophore. The dyes **2** and **3,** relative to the dye **1,** showed similar fluorescence quantum yields (ϕ_{fl}), Table 1. The Table 1 revealed that the dye **2** gave comparable molar extinction coefficients (ε_{max}) at their respective absorption maximum with that of the dye **1** but the dye **3** showed surprisingly enhanced molar extinction coefficients (ε_{max}), almost double in n-heptane compared to that of the dye **2**, indicating the effect of substitution of benzyl groups at 2 and 6- positions of the BODIPY chromophore. We observed that the dye **1** possessed highest fluorescence lifetime of 6.19 ns in ethanol followed by 6.03 ns in n-heptane but the dyes **2** and **3** showing decreased fluorescence lifetimes, 5.9 ns and 5.38 ns in ethanol and 5.32 ns and 4.99 ns in n-heptane, respectively. Correlations of photophysical characteristics and molecular structures of synthesized dyes are discussed in further detail in the theoretical calculations section.

Laser Characteristics. Among different solvents used in this study for understanding photophysical properties of the PM dyes **1**-**3**, we found that normally used ethanol and rarely used n-heptane are suitable for high average power dye laser study. Both ethanol and n-heptane showed good photophysical properties (Table 1) such as

Table 2 Lasing characteristics of the BODIPY dyes **1**-**3**[a] in n-heptane

Dye	λ_L[b] [nm]	η[c] [%]	η_s[d] [%]	Φ_{pd}^{-1}[e]	Φ_{pd}^{-1} of **1** in heptane/ Φ_{pd}^{-1} of **1** in EtOH	Φ_{pd}^{-1} of **2**or **3**/ Φ_{pd}^{-1} of **1**
1	-	-	-	1.67×10^3[f]	82.03	-
	552	16.5	15.3	1.37×10^5		
2	546	12.4	13.4	2.79×10^5	-	2.04
3	547	11.3	12.3	5.27×10^5	-	3.85

[a]Different concentrations of the dyes were used to maintain the O.D.values of their solution at ~1 and ~2.5 (1 mm cell) at pump wavelength 532 nm for narrow band laser and photostability study respectively; [b]The wavelength at which the dye showed maximum lasing efficiency (Error: ±1%); [c]Narrow band peak lasing efficiency; [d]slope efficiency (Error: ±1%); [e]Photostability determined under non-lasing conditions; [f]Photostability of the dye **1** in ethanol under non-lasing conditions taken from our work[33] in the same setup.

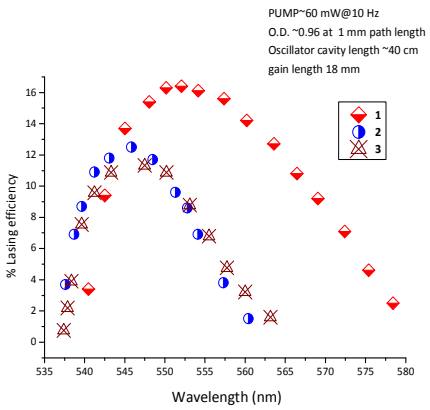

Fig. 4 Narrow-band laser gain curve of the PM dyes **1-3** in n-heptane, determined by using these as gain media in a constructed grazing-incidence-grating (GIG) dye laser transversely pumped with 532 nm irradiation of a Q-switched pulsed (10 Hz) Nd:YAG laser.

high fluorescence yield (ϕ_{fl}) of the dyes **1**-**3** as well as low inflammability (b.p. 78 °C and 98 °C, respectively), viscosity (1 cp and 0.5 cp @ 20 °C, respectively) and toxicity, suitable for handling a large amount of flowing dye solution and maintaining a turbulent flow profile with a thinner boundary layer in the dye flow channel (typically 0.3 to 1 mm width) of such dye lasers. Interestingly, in comparison to ethanol, n-heptane have shown significantly higher photostability (Table 2) of the widely used laser dye **1** (PM567).Therefore, we have studied narrow band laser properties of the newly synthesized dyes **2**-**3** using n-heptane solvent as gain media in the Nd-YAG (532 nm) pumped dye laser.

The results of laser studies of the PM dyes **1**-**3** in n-heptane are presented in Table 2 and shown in Figs. 4 to 6. The narrow band laser profiles of the dyes **1**-**3** follow the pattern of their respective emission spectra (Fig.3) showing maximum lasing efficiency at particular wavelength (λ_L), characteristic of the dye (Table 2 and Fig. 4). The lasing efficiency values (η) of the dyes **1**-**3** are 16.5%, 12.4% and 11.3%, respectively and laser slope efficiency (η_s) values are 15.3%, 13.4% and 12.3%, respectively at their respective laser maxima (Table 2 and Fig. 5). These results revealed that the N-ethyl carbazole moiety provided slightly negative effect on lasing efficiency and the combination of N-ethyl carbazole at *meso* and benzyl groups at 2 and 6-positions is responsible for further small decrease in lasing efficiency. The decrease in lasing efficiency in case of the dyes **2** and **3** could be accounted to the torsional motions of the N-ethyl carbazole and flexible benzyl groups, contributing to the higher non-radiative decay (see Table 1, column 14) rates.

Photostability characteristics: The quantum yields of photodegradation (Φ_{pd}) or photostability (Φ_{pd}^{-1}) data of the dyes **1**-**3**, in air-equilibrated n-heptane solvent, were measured and calculated under non-lasing conditions (Table 2 and Fig. 6).

It is reported that irradiation with 532 nm led to the degradation of the PM dyes at olefinic site (C7'=C8) and produce non-fluorescent products,[28] leaving shape of its absorption band ($S_0 \rightarrow S_1$) unaltered while gradual decrease in respective peak heights. Therefore, decrease in concentration of dye molecules under exposure to laser irradiation, calculated by measuring the reduction in optical density (OD) of the dye solution at λ_{max}, gave estimate of quantum yield of photodegradation (Φ_{pd}) of the dye in respective solvent. Significantly, we have observed eighty two times enhancement in photostability of the dye **1** in n-heptane compared to that in ethanol. Interestingly, the synthesized dyes **2**-**3** showed further enhanced photostabilities, compared with the dye **1**, in n-heptane (Table 2).

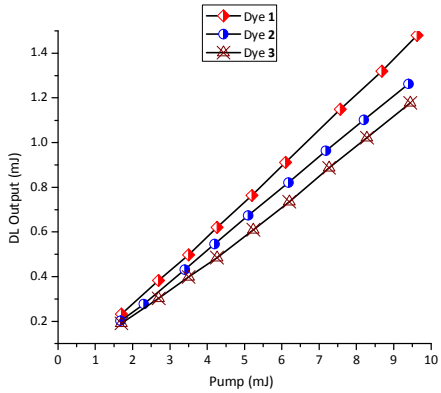

Fig. 5 Comparative slope efficiencies of the dyes **1-3** at the corresponding peak λ_L in n-heptane, determined by pumping with 532 nm irradiation of a Q-switched Nd:YAG laser

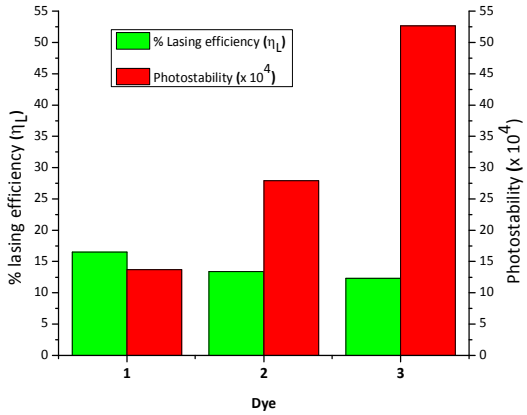

Fig. 6 Narrow band peak lasing efficiencies (%ηL) and photo stabilities (Φ_{pd}^{-1}) of the BODIPY dyes **1**–**3** in n-heptane

The dyes **2** and **3** showed two and four times, respectively, increase in the photostability compared to that of the dye **1** in n-heptane (see Table 2 and Fig. 6) suggesting the positive effect of present modifications on the BODIPY dyes.

It is now well established that the *in situ* generated singlet oxygen ($^1O_2$) is mainly responsible for the breakdown of the PM dye structure as $^1O_2$ adds at the C7'-C8 double bond and forms the peroxo compound. The remarkable enhancement in the photostability of the PM dyes in less polar solvent like n-heptane compared to highly polar solvent ethanol may be attributed to the lower reaction probability of the polar singlet oxygen ($^1O_2$) species with dye molecules in less polar media and vice versa. However, ability of generating $^1O_2$ by PM dyes in solvent environment may vary, which is discussed in the following section.

Generation of $^1O_2$ by dyes: The capacity of generating $^1O_2$ by each PM dye in n-heptane was determined by monitoring the dye-sensitized degradation kinetics of additive DPBF (1, 3-Diphenylisobenzofuran), which possesses high reactivity with $^1O_2$. DPBF essentially traps the produced singlet oxygen ($^1O_2$) through its oxidation.[45,46] The results of our study of generating $^1O_2$ by n-heptane solutions of the dyes are shown in Fig.7. Under the experimental conditions tungsten lamp radiation (λ>495 nm, transmitted through a cut off filter) excited only the PM dye molecules to the S_1 state. This in turn produced dye molecules in the triplet excited state (T_1) depending on the intersystem crossing rate (K_{ISC}) of the dye-solvent system followed by reaction of triplet state (T_1) dye with dissolved oxygen in specific solvent to generate $^1O_2$.

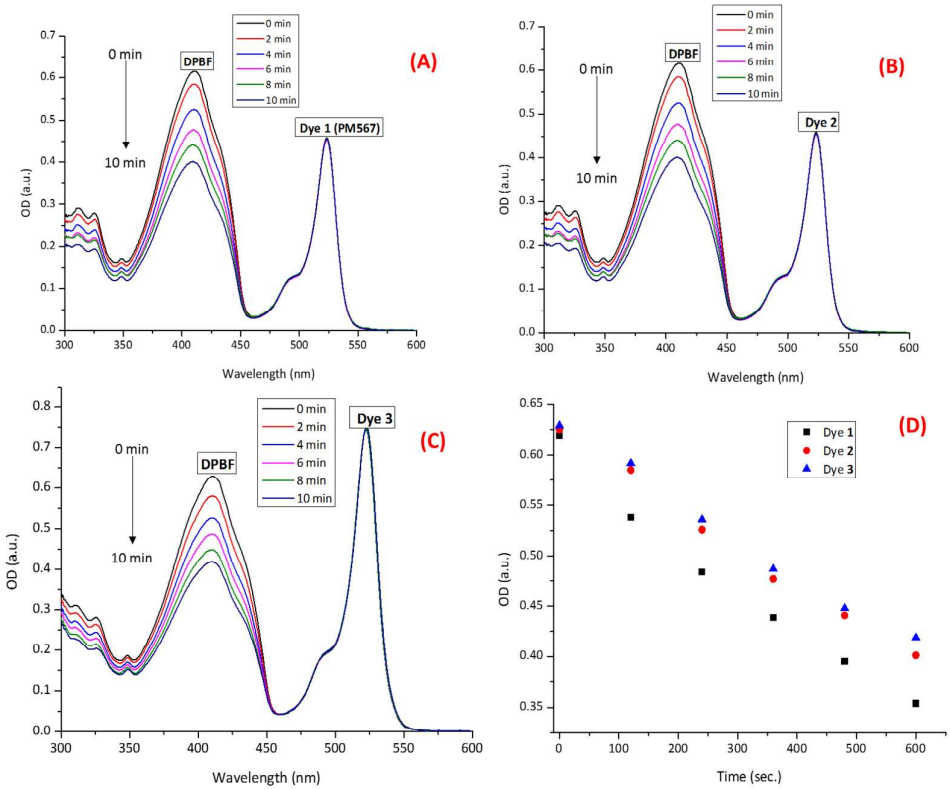

Fig. 7 Absorption spectra of DPBF (50 μM)in presence of the photo-excited dye**s (**5 μM each) in n-heptane**: (**A)-Dye **1**; (B)-Dye **2** and (C)-Dye **3;** after exposure time (0 to 10 min; recorded at 2 min interval) and (D)-Relative rate of $^1O_2$ generation of the dyes **1-3** in n-heptane, determined by measuring time dependent decrease in OD of DBPF at its λ_{max} (412 nm).

The generated $^1O_2$ species reacted mainly with the additive DPBF, since concentration of the DPBF was much higher as well as faster rate of reaction of $^1O_2$ with DPBF.[45] It may be noted that the concentration of DPBF (50 μM) was taken ten times higher than that of the dye (5 μM). This is evident from Fig. 7 which showed no decrease in absorbance of the dye peak during lamp exposure period. However, the absorbance of DBPF was observed to reduce gradually due to reaction with generated $^1O_2$ by PM dyes (Fig. 7). The rate of DPBF consumption with exposure time corresponds to the relative efficiency of $^1O_2$ generation by the particular dye solution. These results illustrated that the dye **3** generated $^1O_2$ at a smaller rate than the dye **2** which in turn generated $^1O_2$ at smaller rate compared to the dye **1** (Fig. 7). So the order of rate of generation of $^1O_2$ is dye **3**<dye **2**<dye **1**, which follows the observed order of photostability of the PM dyes **1-3** (dye **3**>dye **2**>dye **1**) in n-heptane solvent (Table 2 and Fig. 6).

Cyclic voltammetry: Cyclic voltammetry analysis of the BODIPY dyes **1**-**3** showed a reversible peak in each case in the anodic portion of the cyclic voltamograms (Fig. 8), which was assigned to one-electron oxidation of the BODIPY unit. From the Fig.8 and Table 3, it can be seen that the dyes **2** (E_{ox}^0=1.007 V) and **3** (E_{ox}^0=1.075 V) show higher oxidation potential than the dye **1** (E_{ox}^0= 0.997 V), by 10 mV, and 78 mV, respectively. The above data suggest the trend in probability of electron donation capacity of the dyes increases in the order dye**3**<dye **2**<dye **1**, which also supports the observed trend of photo stabilities (dye **3**>dye **2**>dye **1**) of the dyes **1**-**3**.

From larger oxidation potential of the dye **3** relative to that of the dyes **1** and **2** (Table 3), it can be concluded that the benzyl groups at 2 and 6-positions, though not in conjugation with PM core can play important role in decreasing the electron density at reaction site (C7'-C8 double bond), making the dye **3** most stable compared to the dye **2** followed by the dye **1**.

It may be noted that the HOMO of the PM dye and LUMO of the singlet oxygen ($^1O_2$) are involved in the process of photo cleavage of the PM dyes.[48] The energies of HOMO and LUMO and energy gaps, LUMO-HOMO, of the dyes **1**-**3** were determined from their oxidation and reduction potentials. It is apparent that the band gap energy and singlet oxygen generation capacity are directly proportional to each other.[49]

Table 3 Summery of redox potentials and HOMO/LUMO calculations using cyclic voltammetry (CV)

Dye	$E_{1/2}^{Ox}$ [a] (CV) (V)	$E_{1/2}^{Red}$ [a] (CV) (V)	E_{HOMO} [b] (CV) (eV)	E_{LUMO} [c] (CV) (eV)	E_{gap} [d] (CV) (eV)
1	+0.997	-1.157	-5.372	-3.218	2.154
2	+1.007	-1.131	-5.382	-3.244	2.138

3	+1.075	-1.065	-5.450	-3.307	2.140

[a]Half wave potentials of first oxidation and reduction processes (E_{HOMO}(Fc)= -4.78 eV; $E_{1/2}{}^{Ox}$(Fc)=0.405 eV); [b]E_{HOMO}= -4.78 + ($E_{1/2}{}^{Ox}$(Fc) - $E_{1/2}{}^{Ox}$))[47]; [c]E_{LUMO}= -4.78 + ($E_{1/2}{}^{Ox}$(Fc) - $E_{1/2}{}^{Red}$))[47]; [d] E_{gap}= E_{LUMO} - E_{HOMO};CV= Cyclic voltammetry.

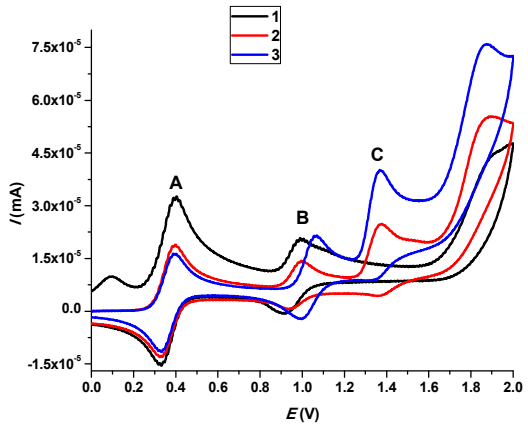

Fig. 8 Cyclic voltamograms of the BODIPY dyes **1**-**3** in acetonitrile at room temperature (A=$E_{ox}{}^{0}$ of Fc/Fc^{+}; B=$E_{ox}{}^{0}$ of BODIPY core; C=$E_{ox}{}^{0}$ of Carbazole core)

The dyes **2** and **3** have got almost similar HOMO-LUMO band gap but the dye **1** has higher band gap compared to the dyes **2** and **3**, which indicates the dye **1** can produce more singlet oxygen compared to the dyes **2** and **3**. The results of $^{1}O_2$ generation using dye sensitized DPBF and cyclic voltammetry experiments illustrated that the dyes **2** and **3** have lower capacity to generate singlet oxygen ($^{1}O_2$) as well as lower reactivity with the generated $^{1}O_2$ in comparison to the dye **1**. The dye **3** showed higher oxidation potential than dye **2,** explaining enhanced photo stability of the dye **3**. Therefore, modifications at either *meso* or both at *meso* and 2 and 6-positions did not alter considerably the photophysical properties of congeners of PM567, but their electronic properties.

Theoretical Interpretations. The BODIPY dyes **1**-**3** possess a compact chromophore with high molar extinction coefficients, which can be used to explore their electronic structures in various solvents by means of DFT and TD-DFT calculations using B3LYP/6-31G(d) level of theory. We have analyzed the absorption and emission characteristics of the PM dyes **1**-**3** and correlated these with the observed laser and photostability properties.

Geometries in ground state and lowest lying excited singlet and triplet states. The dyes **1**-**3** were optimized in their ground (S_0) state, and lowest lying excited singlet (S_1) and triplet (T_1) states with the help of DFT and TD-DFT using B3LYP/6-31G(d) method for all the atoms in vacuum and various organic solvents. For illustration, the results of geometry optimization of the dyes **1**-**3** in n-heptane media are presented in Table 4 (please refer to the Fig. 9 for atom numbering used to explain DFT and TD-DFT parameters). The BODIPY unit found to be perfectly planer in optimized geometries (S_0, S_1 and T_1) of the dyes **1**-**3** with very little displacement (0.6-5.4 Å) of boron atom revealing the effective overlap of *p*-orbitals. In both the dyes **2** and **3**, N-ethyl carbazole at *meso* (C-8) position oriented orthogonally relative to the BODIPY framework with a little twist making an angle of 95.1° and 95.3°, respectively, in the S_0 state

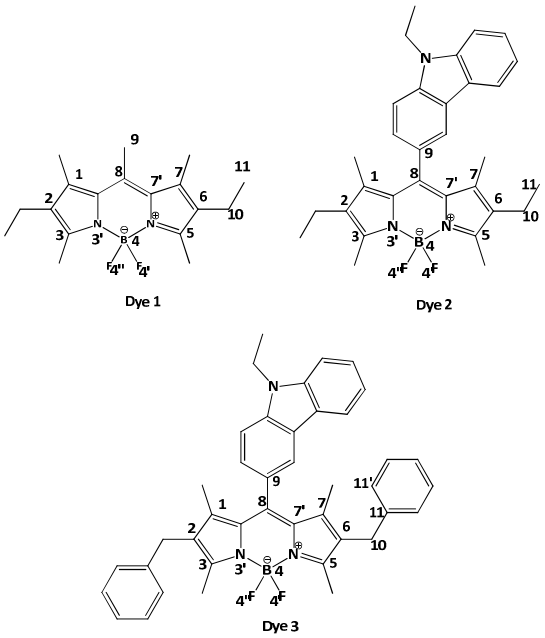

Fig. 9 Atom numbering system presented to explain the DFT and TD-DFT results for the PM dyes **1**-**3**

Further, in the excited state (S_1) the N-ethyl carbazole turn out to be perfectly orthogonal with the BODIPY plane making dihedral angle of 90.9 and 90.8°, respectively. These results signify that the N-ethyl carbazole moiety is not electronically coupled with BODIPY plane in S_0 and S_1states, and thus show negligible influence on the photophysical properties (absorption and emission maxima) of the dyes **2** and **3**. The phenyl rings of 2 and 6-substituents in case of the dye **3** appear to make an angle of 36.2°, 34.4°and 37.5° in S_0, S_1 and T_1 states, respectively. The shortening of the C8-C9 bond by 0.013 Å is observed in case of both the dyes **2** and **3** relative to that of the dye **1** suggested the intramolecular charge transfer from N-ethyl carbazole to BODIPY core**.** Shortening of C10-C11 bond is observed in case of the dye **3** by 0.013 Å relative to that of the dye **2**, supports the alteration of the electronic properties of the BODIPY core as a result of incorporation of benzyl groups at 2 and 6-postions of the BODIPY core.There is negligible change in the other geometrical parameters such as bond lengths, bond angles, dihedral angles etc.(Table 4) when molecules are excited from $S_0 \rightarrow S_1$ state leading to the emission of energy with minimum energy loss (small Stokes shift) which is characteristics of typical BODIPY dyes.[50]

Table 4 shows that the N-ethyl carbazole at *meso* position in the dyes **2** and **3**, in T_1 state, is displaced from its perfectly orthogonal

arrangement with BODIPY core in S_1 state by 25.5° and 24.6°, respectively, allowing the *p*-orbital overlap between the two chromophores (N-ethyl carbazole and BODIPY core) effective which may lead to the pronounced intramolecular charge transfer. Also further shortening of C8-C9 bond in T_1 of the dyes **2** and **3** relative to that of S_1 is observed by 0.013 and 0.011 Å which may also increase the probability of charge transfer between N-ethyl carbazole and BODIPY core. Rest of the geometry parameters like bond lengths, bond and dihedral angles are maintained in T_1 similar to that of S_1, except boron atom in dye **2** and **3** is displaced more by 4.1 ° and 3.6 ° from its perfectly planar arrangement in S_1. Both the processes in T_1 state of the dyes **2** and **3**, that is, rotation of N-ethyl carbazole from its orthogonal arrangement, leading to charge transfer and displacement of boron atom from perfectly planer arrangement in respective S_1 state suggest contribution of non-radiative decay rate (k_{nr}) in the energy loss is more for the dyes **2** and **3** relative to that of the dye **1**.

Table 4 TD-DFT optimized parameters of the dyes **1-3** in its ground (S_0), excited singlet (S_1) and triplet (T_1) states, in n-heptane using B3LYP/6-31G(d) level of theory, (bond lengths are in Å, dihedral angles are in degree °)

Atom no.	Dye 1			Dye 2			Dye 3		
	S_0	S_1	T_1	S_0	S_1	T_1	S_0	S_1	T_1
	Bond lengths								
C1-C2	1.399	1.412	1.512	1.399	1.418	1.419	1.398	1.418	1.419
C2-C3	1.416	1.424	1.372	1.417	1.397	1.397	1.419	1.397	1.397
C3-N3'	1.347	1.349	1.380	1.348	1.371	1.373	1.345	1.371	1.372
N3'-B4	1.552	1.543	1.579	1.553	1.543	1.543	1.556	1.543	1.543
B4-F4'	1.398	1.402	1.396	1.398	1.410	1.409	1.397	1.410	1.410
C7'-C8	1.409	1.423	1.413	1.406	1.424	1.433	1.408	1.424	1.432
C6-C10	1.506	1.498	1.490	1.505	1.506	1.505	1.507	1.506	1.506
C8-C9	1.508	1.504	1.509	1.495	1.486	1.473	1.495	1.486	1.475
C10-C11	1.540	1.545	1.549	1.540	1.540	1.540	1.527	1.526	1.526
	Bond angles								
C3-N3'-B4	125.2	124.8	123.2	125.4	125.0	124.6	125.3	125.0	124.6
N3'-B4-F4'	109.8	109.9	107.7	109.9	110.4	110.3	110.2	110.3	110.3
F4'-B4-F4''	110.0	109.2	110.5	109.9	108.4	108.6	110.1	108.4	108.5
	Dihedral angles								
C2-C3-N3'-B4	0.6	0.1	0.6	1.1	1.3	5.4	1.1	1.3	4.9
C7'-C8-C9-C12	-	-	-	95.1	90.9	64.5	95.3	90.8	65.4
C6-C10- C11-C11'	-	-	-	-	-	-	36.2	34.4	37.5

Table 5 Mulliken charges (e.s.u.) on selected atoms of the dyes **1-3** at their respective optimized ground state geometries, calculated by B3LYP/6-31G(d) level of theory in n-heptane.

Dye	C-1	C-2	C-3	N-3'	B-4	C-7'	C-8	C-9	C-10
1	0.087	0.019	0.316	-0.576	0.693	0.183	0.115	-0.015	-0.056
2	0.088	0.015	0.317	-0.579	0.694	0.215	-0.030	0.020	-0.055
3	0.097	0.007	0.334	-0.581	0.694	0.214	-0.027	0.019	-0.123

Mulliken Charges. The analysis of Mulliken charge distribution over the atoms of the BODIPY chromophore, in solvent n-heptane (Table 5 and Fig. S5-S7(ESI†)), did show considerable variation on the electron densities at different atoms (C-2, C-7', C-8, C-9, and C-10). Changing the C-8 methyl substituent to the N-ethyl carbazole (dye **2**) led to a little increase in the electron density at C-7, but abrupt decrease in the electron density at C-8 was observed which could be the reason for the decrease in the reactivity of the dye **2** with the generated singlet oxygen ($^1O_2$). It may be noted that addition of singlet oxygen ($^1O_2$) at C7'-C8 double bond of the BODIPY chromophore initiates its photodegradation. Also the dye **3,** in which ethyl substituents at 2 and 6-positions of the dye **1** changed to benzyl, showed the abrupt decrease in the electron density at C-2/C-6 and C-10 while effect of N-ethyl carbazole at C-7', C-8 and C-9 was similar. Therefore, though the phenyl rings in benzyl group were not in direct conjugation with BODIPY chromophore, still could alter the electronic properties of the PM moiety such that its photostability increased. At the same time decrease in the lasing efficiencies of the dyes **2** and **3**, compared to that of the dye **1**,could be explained by sharp decrease in the electron densities at C-8 since the N-ethyl carbazole reduced the flow of electrons over PM chromophore. Comparison of Mulliken charges in S_0 and S_1 states of the dyes **2** and **3** revealed no or negligible change in the electron densities over various atoms of PM moiety (Table S1(ESI†)).

TD-DFT excitations and emissions. Further the DFT and TD-DFT (B3LYP/6-31G(d)) method have been employed to get more understanding of the photophysical properties of the synthesized dyes and the results are summarized in Tables 6 and 7. The results suggested no or negligible influence of change in solvent polarity on the photophysical properties of the PM dyes (Table 7), which agree with our experimental observations. The Table 7 revealed that the absorption maxima for the dyes **2** and **3** in all different solvents are centered around 442-447 nm with about 15% deviation from the experimental values of the absorption maxima. In all the studied solvents the vertical excitations of the dyes **2** and **3** were found to associate with the HOMO to LUMO (π to π^*) transition while the oscillator strengths ranged from 0.54 to 0.69. For comparison we have performed the similar calculation for dye **1** also (Table 6)

which showed its absorption maxima slightly blue shifted by about 2-6 nm compared to that of the dye **2** and **3**. The TD-DFT also accounted for the enhanced ε_{max} values of the dye **3** showing its higher oscillator strengths of vertical excitation compared to that of the dye **2** in all the studied solvents. In addition to the normal HOMO to LUMO transition for dyes **2** and **3** (443.4 and 445.1 nm, respectively), the S_0 to S_1 excitations mainly contributed by the HOMO-1 to LUMO transition and located at 447 nm and 456 nm, respectively, in n-heptane with negligible oscillator strengths. These characteristic effects were originated from intramolecular charge transfer characters from *meso* N-ethylcarbazole to BODIPY core. This intramolecular charge transfer may be responsible for their enhanced photostabilities compared to that of the dye **1** (the point of charge transfer is also explained later in section of frontier molecular orbital energies).

The energy optimized structures of S_1 were subjected again to the single point energy calculations using TD-DFT in order to get calculated emission spectra. Consistent with the experimental observations, the calculated emission spectra also suggested that there is no influence of change in solvent polarity, on the vertical emissions of the dyes **2** and **3**. The TD-DFT emission maxima for the dye **2** in various solvents are centered at 449.8 nm to 550.8 nm with oscillator strength in the range 0.43-0.53. For highly polar solvents such as acetonitrile, DMF, DMSO, MeOH, EtOH, acetone, etc. the emissions for the dye **2**were found to associate with LUMO to HOMO-1 transition. Conversely, in case of solvents of lower polarities like ethyl acetate, chloroform, 1, 4-dioxane and n-heptane, the emissions for the dye **2** were found to associate with LUMO to HOMO. Similarly the TD-DFT emissions for the dye **3** in various solvents are centered at 450.1 nm to 452.9 nm in various solvents with enhanced oscillator strengths (0.52-0.59) compared to the dye **2** (Table 7). Consistent with the observation of low Stokes shifts in the range of 506 cm^{-1} to 360 cm^{-1} for the dyes **2** and **3**, TD-DFT also suggested smaller Stokes shifts of 367 to 250 cm^{-1}. Thus, TD-DFT calculation also accounts to the experimentally observed lower Stokes shifts of the dyes **2** and **3** (Table 7). In case of ethyl acetate and chloroform solvents, the dye **3**, unlike the dye **2,** shows emissions associated with the LUMO to HOMO transitions.

Table 6 Calculated light-absorption parameters of the PM dyes **1-3** in ethanol and n-heptane solvents using TD-DFT (B3LYP/6-31G(d)) PCM method

Dye	Ethanol			n-Heptane		
	$E_{S0\rightarrow S1}$ [a] (eV)	λ_{abs} [b] (nm)	f [c]	$E_{S0\rightarrow S1}$ (eV)	λ_{abs} (nm)	f
1	2.83	439	0.5933	2.81	441	0.6202
2	2.80	443	0.5557	2.80	443	0.5241
3	2.79	445	0.6504	2.79	445	0.6890

[a]Energy required for vertical transition from the ground (S_0) to excited state (S_1); [b]Absorption wavelength; [c]Oscillator strength of vertical excitation

Table 7 TD-DFT absorptions and emissions parameters of the dyes **2** and **3** in various solvents.

Solvent	λ_{abs} [a] (nm)	TD-B3LYP/6-31G(d)-Absorptions				λ_{em} [f] (nm)	$\Delta\nu$ [g] (nm)	TD-B3LYP/6-31G(d)-Emissions				
		λ_{abs} [b] (nm)	f [c]	D [d] (%)	Major contribution [e]			λ_{em} [h] (nm)	$\Delta\nu$ [i] (nm)	f [i]	D [k] (%)	Major Contribution
Dye 2												
MeCN	519	442.5	0.5490	14.7	H→L (91.50%)	533	506	449.8	367	0.4457	15.6	L→H-1 (76.41%)
DMF	522	444.9	0.5725	14.8	H→L (92.40%)	535	465	452.2	363	0.4791	15.5	L→H-1 (81.08%)
DMSO	522	444.6	0.5691	14.8	H→L (92.26%)	536	500	451.7	354	0.4741	15.7	L→H-1 (78.93%)
MeOH	519	442.0	0.5446	14.8	H→L (91.34%)	532	471	449.4	373	0.4395	15.5	L→H-1 (75.82%)
EtOH	521	442.9	0.5557	15.0	H→L (91.86%)	533	432	450.2	366	0.4561	15.5	L→H-1 (76.78%)
Acetone	519	443.0	0.5545	14.7	H→L (91.75%)	532	471	450.2	361	0.4559	15.4	L→H-1 (79.28%)
EtOAc	521	443.2	0.5687	14.9	H→L (92.51%)	532	397	449.8	331	0.4852	15.4	L→H (76.86%)
$CHCl_3$	525	445.3	0.5898	15.2	H→L (93.11%)	537	426	451.6	313	0.5185	15.9	L→H (82.51%)
1, 4-Dioxane	523	444.6	0.5711	15.0	H→L (89.08%)	535	429	450.8	309	0.5332	15.7	L→H (85.10%)
Heptane	523	443.4	0.5241	15.2	H→L (81.92%)	535	429	449.7	316	0.5262	15.9	L→H (84.66%)
Dye 3												
MeCN	520	444.7	0.6431	14.5	H→L (90.16%)	532	434	450.9	309	0.5258	15.3	L→H-1 (77.23%)
DMF	522	447.0	0.6667	14.4	H→L (91.02%)	534	430	452.9	291	0.5670	15.2	L→H-1(80.67%)
DMSO	524	446.7	0.6623	14.8	H→L (90.77%)	536	427	452.6	292	0.5584	15.6	L→H-1 (79.99%)
MeOH	520	444.3	0.6389	14.6	H→L (89.99%)	532	434	450.4	305	0.5188	15.3	L→H-1 (76.61%)
EtOH	521	445.1	0.6504	14.6	H→L (90.59%)	532	397	451.1	299	0.5406	15.2	L→H-1(78.48%)
Acetone	521	445.1	0.6412	14.6	H→L (90.69%)	531	361	450.9	289	0.5433	15.1	L→H-1(78.65%)
EtOAc	521	445.1	0.6709	14.6	H→L (92.18%)	532	397	450.7	279	0.5210	15.3	L→H-1(76.29%)
$CHCl_3$	523	447.0	0.6924	14.5	H→L (92.89%)	535	429	452.2	257	0.5644	15.5	L→H-1(79.51%)
1, 4-Dioxane	522	446.0	0.6982	14.6	H→L (92.59%)	533	395	451.0	249	0.5902	15.4	L→H (79.25%)
Heptane	522	445.1	0.6890	14.7	H→L (91.80%)	532	360	450.1	250	0.5831	15.4	L→H (79.88%)

[a]Experimental maximum absorption wavelength; [b]TD-B3LYP/6-31G(d) absorption maximum wabelength; [c]Oscillator strength of vertical excitation; [d]Deviation from the observed absorption maximum; [e]Major electronic transition; [f]Experimental maximum emisson wavelength; [g]Observed Stokes shift; [h]TD-B3LYP/6-31G(d) emission maximum wabelength; [i]TD-DFT Stokes shift; [j]Oscillator strength of vertical emission; [k]Deviation from the observed emission maximum; H=HOMO; L=LUMO

The fluorescence quantum yields and comparison of radiative (Kr) rate constants. The fluorescence quantum yield (ϕ_{fl}) from an S_1 state to S_0 state can be correlated with the radiative (k_r) and non-radiative (k_{nr}) rate constants by following equation,

$$\phi_{fl} = \tau_{fl} k_r = \frac{k_r}{k_r + k_{nr}} \qquad (1)$$

Where τ_{fl} is fluorescence life time.

The fluorescence quantum yields (ϕ_{fl}) are affected by competition between the k_r and $k_{nr.}$ Therefore, a small value of k_{nr} and a large value of k_r are necessary for molecule to be more fluorescent.

The S_1–T_1 intersystem crossing rate (k_{ISC}) plays a crucial role in the emission process. Therefore, we focus on the k_{ISC} to get further insight into the different k_r of the dyes **1**-**3** in heptane media. The calculated T_1 energy parameters relative to that of S_1 along with the experimental fluorescence quantum yields (ϕ_{fl}) and radiative (k_r) and non-radiative (k_{nr}) rate constants in n-heptane media are presented in Table 8. A qualitative explanation of the K_{ISC} can be accomplished as a function of the energy separation between the singlet S_1 and the closest triplet Tn,[51,52] as the K_{ISC} exponentially decreases as the singlet–triplet gap ($\Delta E_{S1\text{-}Tn}$) increases.[53,54]

The minimum $\Delta E_{S1\text{-}T1}$ favors the enhancement in k_{ISC}, leading to an increased k_r thus the ϕ_{fl}. Table 8 shows that the $\Delta E_{S1\text{-}T1}$ is relatively smaller for the dyes **2** and **3**, 1.757 eV and 1.759eV respectively, compared with the dye **1** (2.257 eV), which accounts for the experimentally observed larger k_r of the dyes **2** and **3** (Table 8). Also from table 8 it can be seen that the trend of $\Delta E_{S1\text{-}T1}$ for dyes **1**-**3** (dye **1**> dye **3**> dye **2**) agrees with the experimentally observed trend in k_r, that is dye **2**> dye **3**> dye **1**.

From the above discussion we can conclude that the dyes show ϕ_{fl} owing to its smaller k_{nr}, though the dyes **2** and **3** possess larger k_r compared the dye **1.** Still dye **2** show similar ϕ_{fl} and dye **1** show lower compared to that of the dye **1** which can be attributed to their larger non-radiative (k_{nr}) rate contents compared to the dye **1** (Table 8).

Table 8 Calculated emitting energy (E_{S1} and E_{T1}, in eV), singlet–triplet splitting energy (ΔE_{S1-T1}, in eV), along with the experimental quantum yield (ϕ_{fl}), the radiative (k_r) and the non-radiative (k_{nr}) rate (10^8 s^{-1}) constants

Dye	E_{S1}	E_{T1}	$\Delta E_{S1\text{-}T1}$	ϕ_{fl}	k_r	K_{nr}
1	2.649	0.3924	2.257	0.98	1.63	0.033
2	2.469	0.7121	1.757	0.98	1.84	0.037
3	2.377	0.6184	1.759	0.89	1.76	0.22

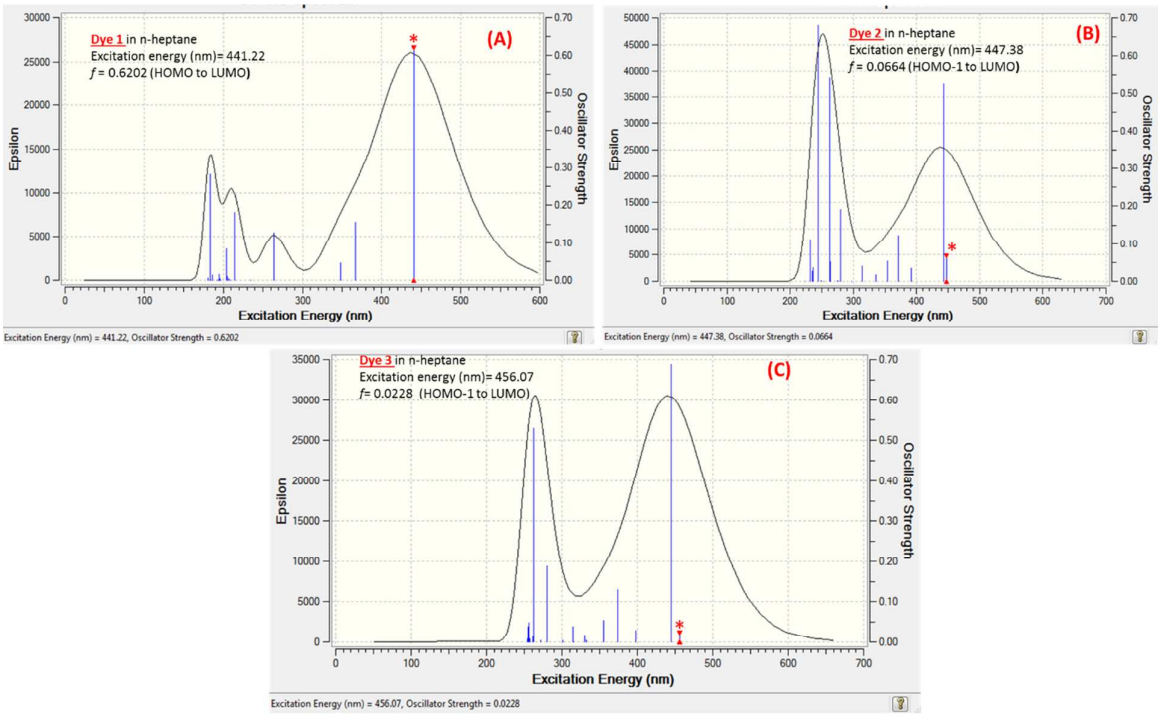

Fig. 10 The simulated (TD-DFT) absorption spectra for the dyes **1-3** in n-heptane media; (A) Dye **1**; (B) Dye **2**; (C) Dye **3.** (Where *f* represents Oscillator Strength)(Note: Markings with star (*) represents mentioned transition).

Dipole moments. Electronic excitation of dye molecule produces redistribution of polarizable π-electrons due to intramolecular charge transfer (ICT), which cause the change in the dipole moment in the excited state. Knowledge on dipole moments of the dye molecule in the ground (S_o) and excited (S_1, T_1 etc.) states are useful to extract parameters like molecular polarizability and to assess the

electron density distribution in the S_1 and T_1 states. The calculated dipole moments of the dye **1** in ethanol and n-heptane along with that of the dyes **2**-**3** in solvents of different polarities are summarized in Tables 9 and S2 (ESI†). The TD-DFT calculations revealed a minimum change in dipole moments of the S_0 and S_1 states of the dyes **2**-**3** in different solvents of various polarities, which support the experimentally observed weak solvatochromism. The calculated dipole moments of the dyes **2**-**3**, both in the ground (μ_0) and the excited singlet (μ_1) states, were larger compared to that of the dye **1** (Table 9), proposing better polarizability of the dyes **2** and **3**.With the decrease in solvent polarity from DMSO to n-heptane, the dipole moments of the S_0 and S_1 states of the dyes **2**-**3** were found to decrease (Table S2(ESI†)) which suggested poor polarization of the PM dyes in less polar solvents like dioxane and heptane. The poor polarizability of the PM dyes in solvents of lower polarities compared to the solvents of higher polarities could be a reason for their enhanced photostability in n-heptane than that in ethanol. This may be associated to more uniform distribution of electronic charges over PM core in case of lower polarity solvents and thus reducing their probability of electron donation to the singlet oxygen ($^1O_2$) species.

Table 9 Ab initio calculated parameters of the PM dyes **1-3** in ethanol and n-heptane using TD-DFT (B3LYP/6-31G(d)) method

Dye	Ethanol						n-Heptane					
	E_H[a] (eV)	E_L[b] (eV)	E_H-E_L (eV)	μ_0[c] (Debye)	μ_1[d] (Debye)	$\Delta\mu_{S1\text{-}0}$[e]	E_H (eV)	E_L (eV)	E_H-E_L (eV)	μ_0 (Debye)	μ_1 (Debye)	$\Delta\mu_{1\text{-}0}$
1	-5.360	-2.362	2.998	5.7137	5.8945	0.1808	-5.236	-2.261	2.976	4.5632	4.7791	0.2159
2	-5.355	-2.414	2.941	8.3747	9.1530	0.7783	-5.167	-2.235	2.932	7.1437	7.6358	0.4921
3	-5.423	-2.473	2.949	8.4841	9.1725	0.6884	-5.247	-2.307	2.941	7.2641	7.6076	0.3435

[a]Energy of highest occupied molecular orbital (HOMO); [b]Energy of lowest unoccupied molecular orbital (LUMO); [c]Dipole moment in ground state (S_0);[d]Dipole moment in excited state (S_1); [e]Change in the dipole moment

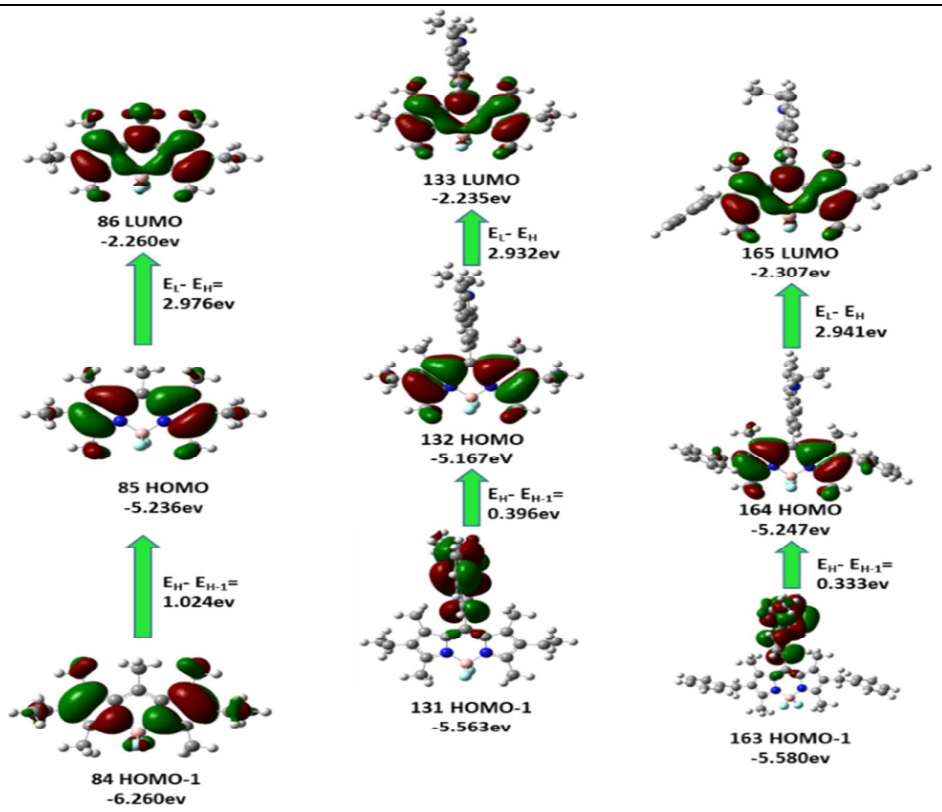

Fig. 11 Frontier molecular orbitals of the dyes **1-3** in n-heptane, calculated by B3LYP/6-31G(d) level of theory (The orbital diagrams are plotted with the contour value of 0.02 a. u.

Frontier Molecular Orbital Energies. Energy levels of the frontier molecular orbitals (FMOs), especially HOMO-1, HOMO, LUMO and LUMO+1, and their spatial distributions can give the idea about behavior of the dye molecules in terms of photophysical properties, lasing properties and photostabilities.

The contour plots of the HOMO-1, HOMO and LUMO of dyes **1**-**3** in n-heptane, calculated byB3LYP/6-31G(d) level of theory, are shown in Fig. 11 and HOMO and LUMO energies and band gaps in ethanol and n-heptane and that of the dyes **2**-**3** in the solvents of different polarities are summarized in Table 9 and Table S2 (ESI†), respectively. Fig. 11 illustrates that in HOMO-1 orbital of the dye **1** the electron density is situated mainly on the BODIPY chromophore, away fromC-7, C-7' and C-8 and very little on B-4. In case of HOMO of the dye **1**, the electron density is localized again on the BODIPY core but completely away from N-3, N-3' and B-4. However, the electron density is distributed almost uniformly over the whole chromophore for LUMO of the dye **1**. This indicated that the HOMO of the PM dye can easily react with the singlet oxygen ($^1O_2$) because the C7'-C8 bond possesses maximum electron density in the HOMO compared to HOMO-1 and LUMO. In case of the dyes **2** and **3**, unlike the dye **1**, the electron density in HOMO-1 is localized only on the *meso* substituent (N-ethyl carbazole) which is transferred to BODIPY core in HOMO and LUMO. This proposes charge transfer from *meso* substituent to the BODIPY core. It may be noted that the C8-C9 bond length was found to be shorter by 0.013 Å in the S_0 as well as S_1 states of the dyes **2** and **3** compared to the dye **1** (see the geometrical parameter section), which also indicated the intramolecular charge transfer from the carbazole moiety to the PM core. HOMO and LUMO of the dyes **2** and **3** show similar results like that of the dye **1**, confirming the involvement of HOMO of the dye **2** and the dye **3** too in the reaction with singlet oxygen ($^1O_2$). From Table 3, Table 9 and Fig. 11 it can be seen that TD-DFT analysis accounts correctly the HOMO-LUMO band gaps as it follows observed trend in cyclic voltammetry study. The dye **1** has higher HOMO-LUMO band gap followed by the dye **3** and then the dye **2**.

Figures 12 to 13 and Table S2 (ESI†) revealed that the dye **3** shows more band gap (HOMO→LUMO) compared to the dye **2** in different organic solvents. Among the series of studied solvents it is observed that for both the dyes **2** and **3** there is a decrease in band (HOMO-LUMO) gap from polar to non-polar solvents. But the band gap between HOMO-1 to HOMO is increased from polar to non-polar solvents which indicated

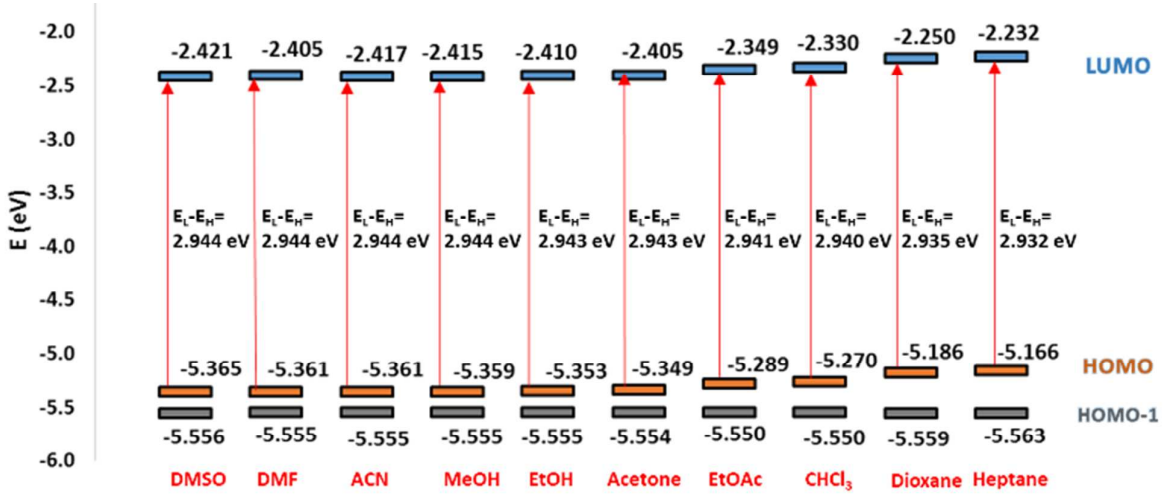

Fig. 12 Energy gaps between HOMO-1, HOMO and LUMO gaps of the dye **2** in various solvents

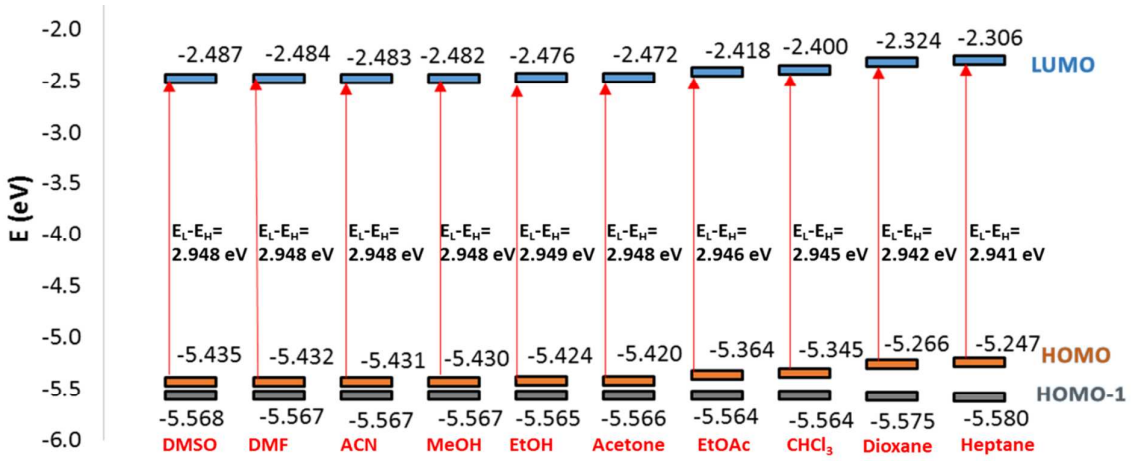

Fig. 13 Energy gaps between HOMO-1, HOMO and LUMO gaps of the dye **3** in various solvents

possibility of vertical emission from LUMO→HOMO-1 is less feasible in case of the solvents of lower polarity (Table 9, Fig. 12 and 13). As the solvent polarity decreases from DMSO to n-heptane, the HOMO as well as LUMO becomes higher in energy with little decrease in band gap. But the energy of HOMO-1 is not much influenced by a change in the polarity resulting to an increase in the band gap (HOMO-1to HOMO). Thus, the LUMO to HOMO-1 transition becomes less feasible with a decrease in solvent polarity.

Experimental Section

General Methods. Laser grade pyrromethene 567 (PM 567) was procured and used without any further purification. The purity of the dye was found to be >99%, as determined with spectroscopic and chromatographic methods. The chemicals and spectroscopic grade solvents were procured and used as such without further purifications unless otherwise mentioned. All the common chemicals were of analytical grade. The solvents were purified by standard procedures. All the reactions were monitored by TLC (thin-layer chromatography) with detection by UV light.The absorption spectra were recorded on commercially procured UV/VIS spectrometer. The emission spectra of PM dyes were recorded on fluorescence spectrophotometer using 10 mm cuvette with 2.5 slit width at 490 nm excitation wavelength.The FT-IR spectra were recorded on FT/IR-4100 Fourier Transform Infrared Spectrometer. HRMS analysis were done using 6550 iFunnel QTOF LC/MS, 1290 infinity Binary pump. Mass spectra were recorded on Finnegan mass spectrometer. ^{1}H NMR, ^{13}C NMR, ^{11}B NMRand ^{19}F NMR spectra were recorded on 500 MHz instrument using TMS as an internal standard.

Synthesis. The two novel PM dyes **2** and **3**, have been synthesized and their molecular structures are illustrated in Fig. 1 along with the structure of the parent dye **1** (PM567). The dye **2** was synthesized by using N-ethyl carbazole aldehyde (**4**) and the well known kryptopyrrole (**A**) (Scheme 1). Also, the dye **3** was synthesized using N-ethyl carbazole aldehyde (**4**) and pyrrole (**8**) (Scheme 2) and instead of DDQ, a milderoxidisingagent, p-chloranil, was used in order to avoid the photocleavage of C8-C9 bond. It is worth mentioning that the pyrrole (**8**) intermediate can be obatined as a pure solid easily in a few minutes from its corresponding salt of carboxylic acid (**7**) at room temperature after simple work up and can be stored in refrigerator for a few weeks.

3-Ethyl-2, 4-dimethyl-1H-pyrrole (A).The pyrrole intermediate (**A**) was synthesized, following the reported[48]protocol in the reference whenever required and used immediately after column purification in the synthesis of the dye **2** (Scheme 1).

9-Ethyl-9H-carbazole-3-carbaldehyde (4).The compound **4** was synthesized from N-ethyl carbazole as white solid (73.7%) by using reported procedure.[55]

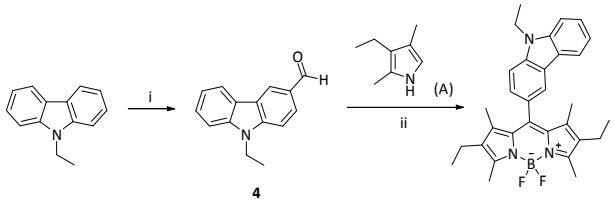

Reagents: i)$POCl_3$/DMF/0-80 ^{o}C/overnight; v)TFA/DCM/2 h/p-chloranil/1.5 h; ii)BF_3:OEt_2/Et_3N/DCM/1.5 h

Scheme 1 Synthesis of the dye **2**

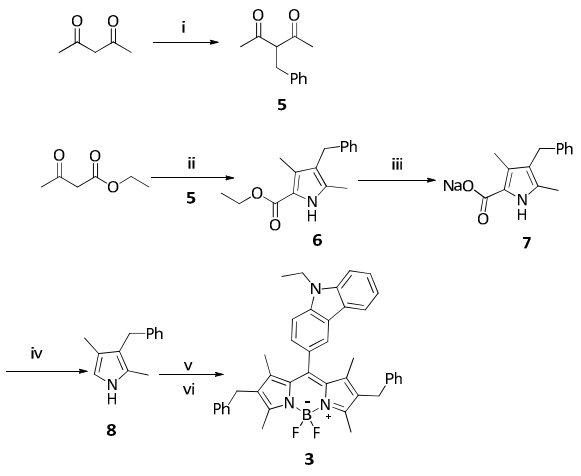

Reagents: i)Benzyl bromide/Na_2CO_3/acetone/reflux/24 h; ii)$NaNO_2$/AcOH, 0-20 °C 12 h/Zn/80 °C/1.5 h; iii)NaOH/EtOH/H_2O/reflux/5 h; iv)TFA/r.t./5 min; v) **4**/TFA/DCM/1 h/p-chloranil/1.5 h; vi)BF_3:OEt_2/Et_3N/DCM/1.5 h.

Scheme 2 Synthesis of the dye **3**

3-Benzylpentane-2, 4-dione (5).To a stirred solution of acetyl acetone (5 g, 0.0499 mol) in acetone (25 mL) at 0 °C was added a sodium carbonate (6.86 g, 0.0648 mol) in portions and the mixture was allowed to stir for 15 min. Then to this was added drop wise solution of benzyl bromide (8.96 g, 0.0524 mol) in acetone (20 mL) for 15 min. Then resulting mixture was allowed to stir at reflux temperature for 24 h. The cooled reaction mixture was filtered to remove solid sodium carbonate, filtrate was concentrated under vacuum and the pale yellow liquid obtained was allowed to stand for 5-6 h. The off white solid was discarded by decantation and obtained product (**5**) as pale yellow liquid. This was used as such without any further purification for next step. Crude yield: 8.37 g, (88%).

Ethyl 4-benzyl-3, 5-dimethyl-1H-pyrrole-2-carboxylate (6).To a solution of ethyl acetoacetate (3.42 g, 0.0263 mol) in acetic acid (12 mL) at 0°C was added drop wise a cold solution of sodium nitrite (2.2 g, 0.0315 mol) in water (10 mL). After stirring the mixture for 12 h at 15-20 °C, to this the compound **5** (5 g, 0.0263 mol) in one portion was added followed by a portion wise addition of zinc dust (3.46 g, 0.0526 mol) while maintaining the temperature below 15 °C. After completion of addition zinc was allowed to react at room temperature with vigorous stirring for 15-20 min and then the mixture was heated at 80 °C for 1.5 h. The reaction mixture was allowed to attain room temperature and poured on to the ice cold water (~500 mL). The precipitated white solid was isolated by filtration; dried and recrystallized from chloroform, which gave **6** as white solid. Yield: 6.12 g, 90.5%. Mp: 127 °C; ^{1}H NMR; (500MHz; $CDCl_3$, TMS): δ 1.35 (t, *J*=7Hz, 3H), 2.18 (s, 3H), 2.22 (s, 3H), 3.76 (s, 2H), 4.3 (q, *J*=7Hz, 2H) 7.09-7.17 (m, 3H), 7.25 (t, *J*=7.5Hz, 2H), 8.63 (bs, 1H, NH); ^{13}C NMR; (500MHz; $CDCl_3$, TMS): δ 10.76, 11.68, 14.58, 29.83, 59.66, 117.01, 120.28, 125.66, 128.01, 128.28, 130.12, 141.17, 161.59; MS (ESI): *m/z* calcd for $(M+H)^+$ $C_{16}H_{20}NO_2$ 258.1; found 257.9.

Sodium 4-benzyl-3, 5-dimethyl-1H-pyrrole-2-carboxylate (7).To a solution of **6** (5 g, 0.0194 mol) in ethanol (20 mL) was added sodium hydroxide (1.55 g, 0.0388 mol) followed by ~0.5 mL water. The resulting mixture was allowed to stir at reflux temperature for 5 h. After completion of reaction, confirmed by TLC, the reaction mixture was allowed to cool at room temperature. The excess ethanol was removed under vacuum and white solid product was isolated after filtration, dried and washed with little ice cold water followed by 5% ethyl acetate in pet ether yielded pure product, **7**, as white solid (4.62 g, 94.6%). ^{1}H NMR (500MHz; D_2O, TMS): δ 2.03 (s, 3H), 2.04 (s, 3H), 3.56 (s, 2H), 7.04-7.08 (m, 3H), 7.18 (t, *J*=7.5Hz, 2H); ^{13}C NMR (500MHz; $CDCl_3$, TMS): δ 11.06, 11.31, 31.06, 118.01, 120.27, 124.18, 124.29, 125.73, 128.38, 128.53, 142.79, 167.73; IR:cm-1 3340 (NH), 1543, 1496, 1428, 1299, 925, 811, 721.MS (ESI): *m/z* calcd for $(M-23)^-$ $C_{14}H_{14}NO_2^-$ 228.1; found 228.0

3-Benzyl-2, 4-dimethyl-1H-pyrrole (8). To the compound **7** (4 g, 0.0159 mol) in 50 mL round bottom flask was added trifluoroacetic acid (6 mL) at room temperature under N_2 atmosphere and stirred for 5 min. Then to this was added 20 mL chloroform and washed immediately with cold water followed by twice with saturated sodium bicarbonate solution. Then the organic layer was dried on sodium sulphate and solvent was evaporated which upon cooling furnish **8** as off white to light brown solid (1.8 g, 61%) which was stored in refrigerator and used for next step without further purification. Mp: 72 °C; ^{1}H NMR (500 MHz; $CDCl_3$, TMS): δ 1.96 (s, 3H), 2.18 (s, 3H), 3.78 (s, 2H), 6.44 (s, 1H), 7.16 (d, *J*=7.5Hz, 3H), 7.20-7.24 (m, 2H), 7.61 (bs, 1H, NH);^{13}C NMR (500MHz; $CDCl_3$, TMS): δ 10.56, 11.48, 30.22, 112.95, 125.26, 125.35, 126.38, 128.07, 128.16, 128.18, 142.27; IR: cm^{-1} 3415, 1604, 1490, 1452, 1351, 1226, 1155; MS (ESI): *m/z* calcd for $(M+H)^+$ $C_{13}H_{16}N$ 186.1; found 186.3.

2, 6-Diethyl-4, 4-difluoro-1, 3, 5, 7-tetramethyl-8-(9-ethyl-9H-carbazol-3-yl)-4-bora-3a, 4a-diaza-s-indecene (2). A stirred mixture of compound **A** (0.662 g, 5.37 mmol), **4** (0.3 g, 2.68 mmol) in dry CH_2Cl_2 (250 mL) was degassed using dry N_2 for 5 min. Then a drop of trifluoroacetic acid was added maintaining dry atmosphere and stirring at r.t. for 2 h. Then the p-chloranil (0.665g, 2.68 mmol) was added to the resulting reaction mixture, and stirring was continued for another 1.5 h. Then dichloromethane was removed using rotary evaporator and the dark red solid obtained was washed twice with pet ether in order to get rid of non-polar impurities. Then the dried red solid was dissolved in fresh dry CH_2Cl_2 (250 mL) and the mixture was treated with trimethylamine (1 mL) and stirred for 15 min. Finally, $BF_3{\cdot}Et_2O$ (1.32 mL, 10.74 mmol) was added to the mixture with vigorous stirring in portions over 10 min, and the solution stirred at room temperature for 1 h. The resulting greenish mixture was washed with 2N NaOH, water, and brine and dried on sodium sulphate. Removal of the solvent in vacuum followed by silica gel column chromatography of the residue using hexane−ethyl acetate as eluent furnished **2** (394 mg, 29.5%) as dark orange solid. ^{1}H NMR (500 MHz, $CDCl_3$, TMS): δ 0.98 (t, *J*=7.5Hz, 6H), 1.22 (s, 6H), 1.52 (t, *J*=7Hz, 3H), 2.29 (q, *J*=7.5Hz, 4H), 2.56 (s, 6H,), 4.45 (q, *J*=7Hz, 2H) 7.27 (t, *J*=7.5, 1H), 7.34 (t,

J=1.5 and 7.5Hz, 1H), 7.51 (m, 3H), 7.99 (t, *J*=1.5Hz, 1H), 8.08 (t, *J*=7.5, 1H); ^{13}C NMR (500 MHz, $CDCl_3$,TMS): *δ*11.93, 12.49, 13.82, 14.64, 17.08, 37.81, 108.78, 108.93, 119.21, 120.29, 120.60, 122.68, 123.33, 125.64, 125.96, 126.18, 131.60, 132.55, 138.67, 139.88, 140.33, 141.57, 153.28; HRMS (ESI): *m/z* calcd for $(M+H)^+$ $C_{31}H_{35}BF_2N_3$ 498.2894; found 498.2893.

2, 6-Dibenzyl-4, 4-difluoro-1, 3, 5, and 7-tetramethyl-8-(9-ethyl-9H-carbazol-3-yl)-4-bora-3a, 4a-diaza-s-indecene (3). Following the similar procedure as described for the dye **2**, the dye **3** (540 mg, 34%), dark orange solid, was prepared from pyrrole (**8**)(0.952 g, 5.11 mol) and aldehyde (**4**), (0.572 g 2.56 mol); ^{1}H NMR, (500 MHz, $CDCl_3$, TMS): *δ*1.23 (s, 6H), 1.48 (t, J=7.5Hz, 3H), 2.53 (s, 6H), 3.69 (s, 4H), 4.42 (q, *J*=7.5Hz, 4H), 7.06 (d, *J*=2.5Hz, 4H), 7.15 (t, *J*=7.5Hz, 2H), 7.22-7.28 (m, 5H), 7.36 (dd, *J*=1.5 and 8.5Hz, 1H), 7.46-7.54 (m,3H), 8.02 (d, *J*=1.5Hz, 1H), 8.08 (d, J=7.5Hz, 1H); ^{13}C NMR (500 MHz, $CDCl_3$,TMS): *δ*12.44, 12.90, 13.79, 29.67, 37.79, 108.79, 109.02, 119.24, 120.24, 120.63, 122.60, 123.35, 125.56, 125.65, 125.92, 126.25, 127.99, 128.39, 129.13, 131.85, 139.91, 139.96, 140.12, 140.33, 142.30, 154.29; HRMS (ESI): *m/z* calcd for $(M+H)^+$ $C_{41}H_{39}BF_2N_3$ 622.3207; found 622.3191

Photophysical studies. The absorption and emission spectra of the dyes in different solvents were measured using a 10 mm path length quartz cuvette. The relative fluorescence quantum yields (ϕ_{fl}) of the dyes **2** and **3**, using the standard dye **1** as reference at 490 nm excitation wavelength, and their corresponding molar extinction coefficients (ε_{max}) were determined. The fluorescence lifetimes of the dyes **1-3** were determined by time resolved fluorescence measurements carried out with an LED-based time-correlated single photon-counting (TCSPC) spectrometer. The fluorescence decays were measured with a 390 nm LED (1 MHz) excitation source and a TBX4 detection module coupled to a PMT. Following de-convolution analysis of the fluorescence decays, the time resolution of the present setup was around 50 ps. All the measurements were carried out at ambient temperature (298±1 K), maintained with a microprocessor based temperature controller.

Lasing studies. The lasing studies of dyes **1–3** in n-heptane were carried out by using a constructed narrow-band dye laser setup, transversely pumped by the second harmonic (at 532 nm) output of a Q-switched Nd:YAG laser at a repetition rate of 10 Hz with a pulse energy of around 7 mJ and fwhm of 5–7 ns. All the laser data for the PM dyes in n-heptane were measured by using the same dye laser setup, which is schematically shown in Fig. S8 (ESI†) in the supporting information. The dye laser was constructed with a grazing-incidence-grating (GIG) configuration (with a grating of 2400 lines mm^{-1}) and a 25 X 4-prisms pre-expander. The tuning curve of each dye solution was obtained by scanning the wavelength of the dye laser through the gain profile of the dyes and measuring the wavelengths by a wavemeter (Angstrom WS-6) and average pump and dye laser powers with the power meter (OPHIR). To determine the pump laser threshold (L_T) and slope efficiency (η_s) of each dye solution, the input pump energy was varied and the lasing output of each of the dye solution at the peak of the corresponding gain curve was determined and plotted as a function of pump energy.

Photostability study. The quantum yield of the photo degradation (Φ_{pd}) of the dyes is defined as the probability of the decomposition of the dye molecules by the absorbed pump photons. The photo stability (Φ_{pd}^{-1}) is the inverse of the Φ_{pd} value. A known quantity of dye solution (2.5 mL) in a dye laser cuvette was exposed to pump energy of 6.7-7.2 mJ at 532 nm for a set period of time. The concentration of the dye solution was chosen such that the pump beam was totally absorbed within the dye solution in the cuvette during the exposure of 3-4 h. The solution was constantly stirred with a teflon-coated magnetic stirrer to avoid local heating. The number of photodegraded dye molecules in the exposed volume of the dye solutions was quantitatively estimated from the absorbance at the corresponding λ_{max} before and after photo exposure for a set period of time. The pump energy was measured periodically by the power meter. The reflection loss of the pump beam on incident surfaces of the dye cell was considered for calculating the absorbed cumulative pump photons.

Generation of $^1O_2$ by dyes: The capacity of generating reactive singlet oxygen ($^1O_2$) molecules by photo excited dyes in n-heptane was comparatively determined by measuring the gradual reduction in peak absorbance of the $^1O_2$ quencher DPBF, used as additive, as a function of lamp exposure time. For this, 3 mL of air equilibrated solvent containing a mixture of DPBF (50 µM) and PM dye (5 µM) in 10 mm path length quartz cell, was irradiated at room temperature for a duration of 10 min using a 40 W tungsten lamp aided by a cut off (λ<495 nm) filter. The lamp was driven by a voltage stabilized power supply. Thus solution of the dye and DPBF was irradiated by the visible light emitting wavelengths higher than 495 nm only. During this process, respective PM dye (λ_{abs} maxima 518-523 nm) was excited only and generated $^1O_2$, which reacted primarily with DPBF due to higher reactivity and concentration of the latter (10 times more than dye). The extent of decrease in absorbance of DPBF in the irradiated dye solution as a function of lamp exposure time was a measure of rate of generation of $^1O_2$ by a particular PM dye solution. The progressive decrease in absorbance of DPBF was measured at its λ_{abs} maximum (412 nm) at various fixed intervals (2 min).

Electrochemical studies. Cyclic voltammetry was performed at 25 ^{0}C in deoxygenated acetonitrile containing 0.1 M $TBAPF_6$ (tetra butyl ammonium hexafluorophosphate) and a dye concentration of 0.6-1 mM. The glassy carbon (2 mm diameter) was used as working electrode, platinum wire as a counter electrode and standard calomel electrode as a reference electrode with ferrocene (1 mM) as an internal standard. The redox potentials were standardized with ferrocene (Fc) as the internal reference and referenced to SCE by taking E^0 (Fc/Fc^+) = +0.405 V versus SCE.

Computational details. All the computations were performed using the Gaussian 09 program package.[56] The ground state (S_0) geometry of the dyes was optimized using density functional theory (DFT)[57] method. The first excited (S_1) and triplet excited (T_1) states were optimized using time dependent density functional theory (TD-DFT). The functional used was B3LYP, (the B3LYP combines Becke's three parameter exchange functional (B3)[58] with the nonlocal correlation functional by Lee, Yang and Parr (LYP).[59] The basis set used in both, DFT and TD-DFT methods for all the atoms was 6-31G(d). In order to verify whether the optimized structures have minimum energy, frequency computations were performed at the same level of theory. The vertical excitation energies and oscillator strengths were obtained for the twenty lowest $S_0 \rightarrow S_1$ transitions at the optimized ground state equilibrium geometries by using the Time Dependent Density Functional Theory (TD-DFT) using the same hybrid functional and basis set.[60–67] To obtain their minimum energy geometries (which correspond to the emissive state) the low-lying first singlet (S_1) and triplet (T_1) excited states of the dyes were relaxed using the TD-DFT. The emission wavelengths and oscillator strengths were obtained for the ten lowest $S_1 \rightarrow S_0$ transitions at the optimized excited state equilibrium geometries by using the TD-DFT with the same hybrid functional and basis set.[67] The frequency computations were also carried out at the same level of theory on the optimised geometry of the first excited state of the dyes. All the computations in the various solvents were carried out using the Self-Consistent Reaction Field (SCRF) under the Polarisable Continuum Model (PCM)[68,69]. The electronic absorption spectra, including wavelengths, oscillators strengths, and main configuration assignment, were systematically investigated using TD-DFT with PCM model on the basis of the optimized ground structures.

Conclusions

We have investigated the laser performances and photostabilities of the PM dyes including the commercial laser dye, PM567, and observed remarkably enhanced photostability of the PM dyes in n-heptane compared to that in ethanol for PM567. The two novel congeners showed good lasing efficiencies and increased photostability in n-heptane compared to the PM567. The results of the cyclic voltammetry supports the enhanced photostabilities of the new congeners compared to that of the PM567. Extensively studied the photophysical properties of the new PM dyes experimentally and structural, photophysical and electronic properties by means of DFT and TD-DFT in the solvents of various polarities. These findings will be helpful for the future design and synthesis of efficient and photostable BODIPY laser dyes.

Acknowledgements

Authors thank Dr. V. Sudarshan, Chemistry Division, BARC for his help in fluorescence lifetime decay measurements. Also we are thankful to Mr. Amol Patil and Prof. B. M Bhange for their help in electrochemistry experiments. One of the authors (KGT) is thankful to the Council of Scientific and Insdustrial Research (CSIR), India for Junior and Senior Research Fellowships.

References

1 R. P. Haugland, *Handbook of Fluorescent Probes and Research Chemicals*, USA, 6th edn., 1996.

2 S. Hattori, K. Ohkubo, Y. Urano, H. Sunahara, T. Nagano, Y. Wada, N. V Tkachenko, H. Lemmetyinen and S. Fukuzumi, *J. Phys. Chem. B*, 2005, **109**, 15368–75.

3 K. Rurack, M. Kollmannsberger, U. Resch-Genger and J. Daub, *J. Am. Chem. Soc.*, 2000, **122**, 968–969.

4 B. Turfan and E. U. Akkaya, *Org. Lett.*, 2002, **4**, 2857–2859.

5 C. Goze, G. Ulrich, L. Charbonniere, M. Cesario, T. Prange and R. Ziessel, *Chem. Eur. J.*, 2003, **9**, 3748–55.

6 P. Oleynik, Y. Ishihara and G. Cosa, *J. Am. Chem. Soc.*, 2007, **129**, 1842–3.

7 F. Li, S. I. Yang, Y. Ciringh, J. Seth, C. H. Martin, D. L. Singh, D. Kim, R. R. Birge, D. F. Bocian, D. Holten and J. S. Lindsey, *J. Am. Chem. Soc.*, 1998, **120**, 10001–10017.

8 M. R. W. Martin P. Debreczeny, Walter A. Svec, *Science (80)*, 1996, **274**, 584–587.

9 T. G. Pavlopoulos, J. H. Boyer, M. Shah, K. Thangaraj and M. L. Soong, *Appl. Opt.*, 1990, **29**, 3885–6.

10 T. G. Paviopoulos, J. H. Boyer, K. Thangaraj, G. Sathyamoorthi, M. P. Shah and M. L. Soong, *Appl. Opt.*, 1992, **31**, 7089–94.

11 S. C. Guggenheimer, J. H. Boyer, K. Thangaraj, M. Shah, M. L. Soong and T. G. Paviopoulos, *Appl. Opt.*, 1993, **32**, 3942–3.

12 J. H. Boyer, A. M. Haag, G. Sathyamoorthi, M.-L. Soong, K. Thangaraj and T. G. Pavlopoulos, *Heteroat. Chem.*, 1993, **4**, 39–49.

13 R. Duchowicz, L. B. Scaffardi, A. Costela, I. García-Moreno, R. Sastre and A. U. Acuña, *Appl. Opt.*, 2003, **42**, 1029.

14 T. G. Pavlopoulos, M. Shah and J. H. Boyer, *Opt. Commun.*, 1989, **70**, 425–427.

15 M. P. O'Neil, *Opt. Lett.*, 1993, **18**, 37.

16 T. G. Pavlopoulos and J. H. Boyer, in *OE/LASE '94*, ed. R. Scheps, International Society for Optics and Photonics, 1994, pp. 231–239.

17 M. Faloss, M. Canva, P. Georges, A. Brun, F. Chaput and J.-P. Boilot, *Appl. Opt.*, 1997, **36**, 6760.

18 A. Costela, I. Garcia-Moreno and R. Sastre, *Phys. Chem. Chem. Phys.*, 2003, **5**, 4745.

19 A. K. Ray, S. Kumar, N. V. Mayekar, S. Sinha, S. Kundu, S. Chattopadhyay and K. Dasgupta, *Appl. Opt.*, 2005, **44**, 7814.

20 F. Lopez Arbeloa, J. Banuelos Prieto, I. Lopez Arbeloa, A. Costela, I. Garcia-Moreno, C. Gomez, F. Amat-Guerri, M. Liras and R. Sastre, *Photochem. Photobiol.*, 2003, **78**, 30–6.

21 J. Bañuelos, F. L. Arbeloa, V. Martinez, M. Liras, A. Costela, I. G. Moreno and I. L. Arbeloa, *Phys. Chem. Chem. Phys.*, 2011, **13**, 3437–45.

22 I. Esnal, G. Duran-Sampedro, A. R. Agarrabeitia, J. Bañuelos, I. García-Moreno, M. A. Macías, E. Peña-Cabrera, I. López-Arbeloa, S. de la Moya and M. J. Ortiz, *Phys. Chem. Chem. Phys.*, 2015, **17**, 8239–47.

23 D. Zhang, V. Martín, I. García-Moreno, A. Costela, M. E. Pérez-Ojeda and Y. Xiao, *Phys. Chem. Chem. Phys.*, 2011, **13**, 13026–13033.

24 A. Burghart, H. Kim, M. B. Welch, L. H. Thoresen, J. Reibenspies, K. Burgess, F. Bergström and L. B.-Å. Johansson, *J. Org. Chem.*, 1999, **64**, 7813–7819.

25 J. Chen, A. Burghart, A. Derecskei-Kovacs and K. Burgess, *J. Org. Chem.*, 2000, **65**, 2900–2906.

26 A. Harriman, G. Izzet and R. Ziessel, *J. Am. Chem. Soc.*, 2006, **128**, 10868–75.

27 C. Goze, G. Ulrich, L. J. Mallon, B. D. Allen, A. Harriman and R. Ziessel, *J. Am. Chem. Soc.*, 2006, **128**, 10231–9.

28 S. Mula, A. K. Ray, M. Banerjee, T. Chaudhuri, K. Dasgupta and S. Chattopadhyay, *J. Org. Chem.*, 2008, **73**, 2146–54.

29 M. D. Rahn, T. A. King, A. A. Gorman and I. Hamblett, *Appl. Opt.*, 1997, **36**, 5862.

30 M. D. Rahn and T. A. King, *Appl. Opt.*, 1995, **34**, 8260–71.

31 G. Jones, S. Kumar, O. Klueva and D. Pacheco, *J. Phys. Chem. A*, 2003, **107**, 8429–8434.

32 *Solid state lasers X : 24-25 January, 2001, San Jose, [California] USA /*, SPIE, Bellingham, Washington :, 2001.

33 K. K. Jagtap, N. Shivran, S. Mula, D. B. Naik, S. K. Sarkar, T. Mukherjee, D. K. Maity and A. K. Ray, *Chem. Eur. J.*, 2013, **19**, 702–708.

34 B. F. Minaev, *Russ. Chem. Rev.*, 2007, **76**, 989–1011.

35 V. Promarak, M. Ichikawa, T. Sudyoadsuk, S. Saengsuwan, S. Jungsuttiwong and T. Keawin, *Thin Solid Films*, 2008, **516**, 2881–2888.

36 P. Moonsin, N. Prachumrak, R. Rattanawan, T. Keawin, S. Jungsuttiwong, T. Sudyoadsuk and V. Promarak, *Chem. Commun. (Camb).*, 2012, **48**, 3382–4.

37 A. Hameurlaine and W. Dehaen, *Tetrahedron Lett.*, 2003, **44**, 957–959.

38 Y. Li, J. Ding, M. Day, Y. Tao, J. Lu and M. D'iorio, *Chem. Mater.*, 2004, **16**, 2165–2173.

39 M. S. Mudadu, A. N. Singh and R. P. Thummel, *J. Org. Chem.*, 2008, **73**, 6513–20.

40 V. Cherpak, P. Stakhira, B. Minaev, G. Baryshnikov, E. Stromylo, I. Helzhynskyy, M. Chapran, D. Volyniuk, D. Tomkuté-Lukšiené, T. Malinauskas, V. Getautis, A. Tomkeviciene, J. Simokaitiene and J. V. Grazulevicius, *J. Phys. Chem. C*, 2014, **118**, 11271–11278.

41 D. Volyniuk, V. Cherpak, P. Stakhira, B. Minaev, G. Baryshnikov, M. Chapran, A. Tomkeviciene, J. Keruckas and J. V. Grazulevicius, *J. Phys. Chem. C*, 2013, **117**, 22538–22544.

42 V. Cherpak, P. Stakhira, B. Minaev, G. Baryshnikov, E. Stromylo, I. Helzhynskyy, M. Chapran, D. Volyniuk, Z. Hotra, A. Dabuliene, A. Tomkeviciene, L. Voznyak and J. V. Grazulevicius, *ACS Appl. Mater. Interfaces*, 2015, **7**, 1219–25.

43 P. E. Kesavan and I. Gupta, *Dalton Trans.*, 2014, **43**, 12405–13.

44 S. L. Yutanova, M. B. Berezin, A. S. Semeikin, E. V. Antina, G. B. Guseva and A. I. V'yugin, *Russ. J. Gen. Chem.*, 2013, **83**, 545–551.

45 N. Adarsh, R. R. Avirah and D. Ramaiah, *Org. Lett.*, 2010, **12**, 5720–3.

46 K. Gollnick and A. Griesbeck, *Tetrahedron*, 1985, **41**, 2057–2068.

47 S. G. Awuah, J. Polreis, J. Prakash, Q. Qiao and Y. You, *J. Photochem. Photobiol. A Chem.*, 2011, **224**, 116–122.

48 S. Mula, A. K. Ray, M. Banerjee, T. Chaudhuri, K. Dasgupta and S. Chattopadhyay, *J. Org. Chem.*, 2008, **73**, 2146–54.

49 R. L. Watley, S. G. Awuah, M. Bio, R. Cantu, H. B. Gobeze, V. N. Nesterov, S. K. Das, F. D'Souza and Y. You, *Chem. Asian J.*, 2015.

50 A. Loudet and K. Burgess, *Chem. Rev.*, 2007, **107**, 4891–932.

51 D. N. Kozhevnikov, V. N. Kozhevnikov, M. Z. Shafikov, A. M. Prokhorov, D. W. Bruce and J. A. G. Williams, *Inorg. Chem.*, 2011, **50**, 3804–15.

52 C.-H. Yang, Y.-M. Cheng, Y. Chi, C.-J. Hsu, F.-C. Fang, K.-T. Wong, P.-T. Chou, C.-H. Chang, M.-H. Tsai and C.-C. Wu, *Angew. Chem. Int. Ed. Engl.*, 2007, **46**, 2418–21.

53 G. Gigli, F. Della Sala, M. Lomascolo, M. Anni, G. Barbarella, A. Di Carlo, P. Lugli and R. Cingolani, *Phys. Rev. Lett.*, 2001, **86**, 167–170.

54 D. Beljonne, J. Cornil, R. H. Friend, R. A. J. Janssen and J. L. Brédas, *J. Am. Chem. Soc.*, 1996, **118**, 6453–6461.

55 G. Bai, J. Li, D. Li, C. Dong, X. Han and P. Lin, *Dye. Pigment.*, 2007, **75**, 93–98.

56 M. J. Frisch, G. W. Trucks, H. B. Schlegel, G. E. Scuseria, M. A. Robb, J. R. Cheeseman, G. Scalmani, V. Barone, B. Mennucci, G. A. Petersson, H. Nakatsuji, M. Caricato, X. Li, H. P. Hratchian, A. F. Izmaylov, J. Bloino, G. Zheng, J. L. Sonnenberg, M. Hada, M. Ehara, K. Toyota, R. Fukuda, J. Hasegawa, M. Ishida, T. Nakajima, Y. Honda, O. Kitao, H. Nakai, T. Vreven, J. A. Montgomery, J. E. Peralta, F. Ogliaro, M. Bearpark, J. J. Heyd, E. Brothers, K. N. Kudin, V. N. Staroverov, R. Kobayashi, J. Normand, K. Raghavachari, A. Rendell, J. C. Burant, S. S. Iyengar, J. Tomasi, M. Cossi, N. Rega, J. M. Millam, M. Klene, J. E. Knox, J. B. Cross, V. Bakken, C. Adamo, J. Jaramillo, R. Gomperts, R. E. Stratmann, O. Yazyev, A. J. Austin, R. Cammi, C. Pomelli, J. W. Ochterski, R. L. Martin, K. Morokuma, V. G. Zakrzewski, G. A. Voth, P. Salvador, J. J. Dannenberg, S. Dapprich, A. D. Daniels, Farkas, J. B. Foresman, J. V Ortiz, J. Cioslowski and D. J. Fox, *Gaussian 09 C.01*, Gaussian Inc., Wallingford CT, 2009.

57 O. Treutler and R. Ahlrichs, *J. Chem. Phys.*, 1995, **102**, 346.

58 A. D. Becke, *J. Chem. Phys.*, 1993, **98**, 1372.

59 R. G. Lee, Chengteh and Yang, Weitao and Parr, *Phys. Rev. B*, 1988, **37**, 785–789.

60 W. J. Hehre, *Acc. Chem. Res.*, 1976, **9**, 399–406.

61 R. Bauernschmitt and R. Ahlrichs, *Chem. Phys. Lett.*, 1996, **256**, 454–464.

62 F. Furche and D. Rappoport, *Computational Photochemistry (Google eBook)*, Elsevier, Amsterdam, 2005.

63 Y. Gabe, T. Ueno, Y. Urano, H. Kojima and T. Nagano, *Anal. Bioanal. Chem.*, 2006, **386**, 621–6.

64 F. Furche and R. Ahlrichs, *J. Chem. Phys.*, 2002, **117**, 7433.

65 J. Leszczynski and M. Shukla, Eds., *Practical Aspects of Computational Chemistry: Methods, Concepts and Applications (Google eBook)*, Springer, 2009.

66 G. Scalmani, M. J. Frisch, B. Mennucci, J. Tomasi, R. Cammi and V. Barone, *J. Chem. Phys.*, 2006, **124**, 94107.

67 K. G. Thorat, H. Bhakhoa, P. Ramasami and N. Sekar, *J. Fluoresc.*, 2015, **25**, 69–78.

68 M. Cossi, V. Barone, R. Cammi and J. Tomasi, *Chem. Phys. Lett.*, 1996, **255**, 327–335.

69 J. Tomasi, B. Mennucci and R. Cammi, *Chem. Rev.*, 2005, **105**, 2999–3093.